Inorganic Chemistry
Cite This: Inorg. Chem. 2019, 58, 11927−11940
Forum Article
pubs.acs.org/IC

Theoretical Studies on Trinuclear $\{Mn^{III}_2Gd^{III}\}$ and Tetranuclear $\{Mn^{III}_2Gd^{III}_2\}$ Clusters: Magnetic Exchange, Mechanism of Magnetic Coupling, Magnetocaloric Effect, and Magneto−Structural Correlations

Thayalan Rajeshkumar, Reshma Jose, Premaja R. Remya, and Gopalan Rajaraman*

Department of Chemistry, Indian Institute of Technology Bombay, Powai, Mumbai 400076, India

Supporting Information

ABSTRACT: Among various applications that are proposed for {3d−4f} clusters, magnetic refrigeration based on the principle of the magnetocaloric effect (MCE) is gaining attention in recent years due to the substantially large MCE values reported for these types of molecules. While various factors play a role in controlling the MCE values, understanding the structural parameters that control the magnetic exchange play a vital role in the development of novel molecules possessing attractive MCE characteristics. In this regard, theoretical tools based on density functional methods are indispensable. In this work, we have employed density functional methods to study the magnetic properties of six $\{Mn^{III}Gd^{III}\}$ clusters. This comprises a trinuclear complex $\{Mn^{III}_2Gd^{III}\}$, $[Mn_2GdO(Piv)_2(dmem)_2(NO_3)_3]$ (dmem = 2-{[2-(dimethylamino)ethyl]methylamino}-ethanol) (**1**), along with four tetranuclear $\{Mn^{III}_2Gd^{III}_2\}$ complexes, $[Mn_2Gd_2O_2(Piv)_8(HO_2CCMe_3)_2(MeOH)_2]$ (Piv = 2,2-dimethylpropanoic acid) (**2**), $[Mn_2Gd_2O_2(Piv)_8(HO_2CCMe_3)_4]$ (**3**), $[Mn_2Gd_2(OH)_2(O_2CPh)_4(NO_3)_2(teaH)_2]$ (tea = triethanolamine) (**4**), and $[Mn_2Gd_2(O)(Piv)_2(hep)_4(NO_3)_4]$ (hep = 2-(2-hydroxyethyl)pyridine) (**5**), and a single-chain compound containing the $\{Mn^{III}_2Gd^{III}_2\}$ core, $[Mn_2Ln_2(OH)(OMe)(hmp)_4(NO_3)_4(O_3SC_6H_4CH_3)_2]_n$ (hmp = 2-hydroxymethylpyridine) (**6**). Here we have evaluated the exchange interactions between Mn^{III} and Gd^{III} ions and $Mn^{III}\cdots Mn^{III}$ ions in trinuclear as well as tetranuclear complexes. Our DFT-computed exchange interaction (J) values reproduce the experimental susceptibility data well, offering confidence in the estimated J values. Our calculations yield a diverse set of J values among these complexes ranging from weak ferromagnetic to moderate antiferromagnetic $\{Mn^{III}\cdots Gd^{III}\}$ coupling. Using orbital overlap and NBO analysis, we have explored the mechanism of magnetic coupling and deciphered the origin of diverse J values noted among these complexes. Particularly, the importance of Jahn−Teller axes of the Mn^{III} ions and its orientation with respect to the nature of coupling is established using the qualitative mechanism derived. The $\{Mn^{III}\cdots Mn^{III}\}$ coupling in all complexes are estimated to be antiferromagnetic, and the consequence of this on the $\{Mn^{III}\cdots Gd^{III}\}$ J values and how this influences the ground-state S values are discussed in detail. Further, we have developed magneto−structural correlations to evaluate the importance of structural parameters that control the $\{Mn^{III}\cdots Gd^{III}\}$ coupling. Our results reveal that Mn−O−Gd bond angles and Mn−O−Gd−O dihedral angles hold the key to the sign and magnitude of the $\{Mn^{III}\cdots Gd^{III}\}$ J values. Further on, utilizing the computed J values, we have estimated the MCE values for these complexes and offer insight into how these two factors are correlated. To this end, our study reveals that the incorporation of anisotropic Mn^{III} ions in the cluster aggregation could lead to respectable MCE values if a suitable ligand design that offers a way to control the direction of the Jahn−Teller axes of Mn^{III} ions is presented.

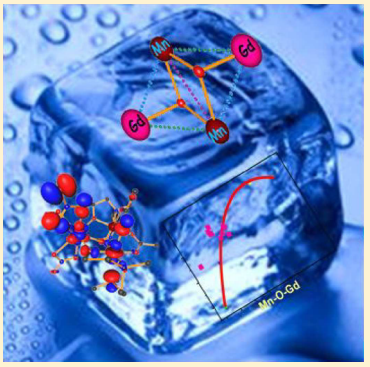

INTRODUCTION

The magnetic refrigeration application is based on the principle of the magnetocaloric effect (MCE), and it is believed to be an alternative for low-temperature cooling applications where He-4, a highly expensive system, is in current use.[1] A large ground state (S) is a common criterion for disk storage and magnetic refrigeration applications, but the second prerequisite on the magnitude of anisotropy differs, where the former application requires the incorporation of a strongly anisotropic transition metal[2] or lanthanide metal ions[3] in the cluster aggregation, while the latter application demands weak or negligible anisotropy. For SMMs, blocking of the spin is required, as this offers a way to store the information, while in MCE applications quicker relaxation is desired to attain faster cooling. The accumulation of states closer to the ground state will result in substantial changes in entropy values upon a variation in the magnetic field (adiabatic demagnetization) which forms the basis for MCE.[4]

Special Issue: Paradigm Shifts in Magnetism: From Molecules to Materials

Received: May 22, 2019
Published: August 15, 2019

DOI: 10.1021/acs.inorgchem.9b01503
Inorg. Chem. 2019, 58, 11927−11940

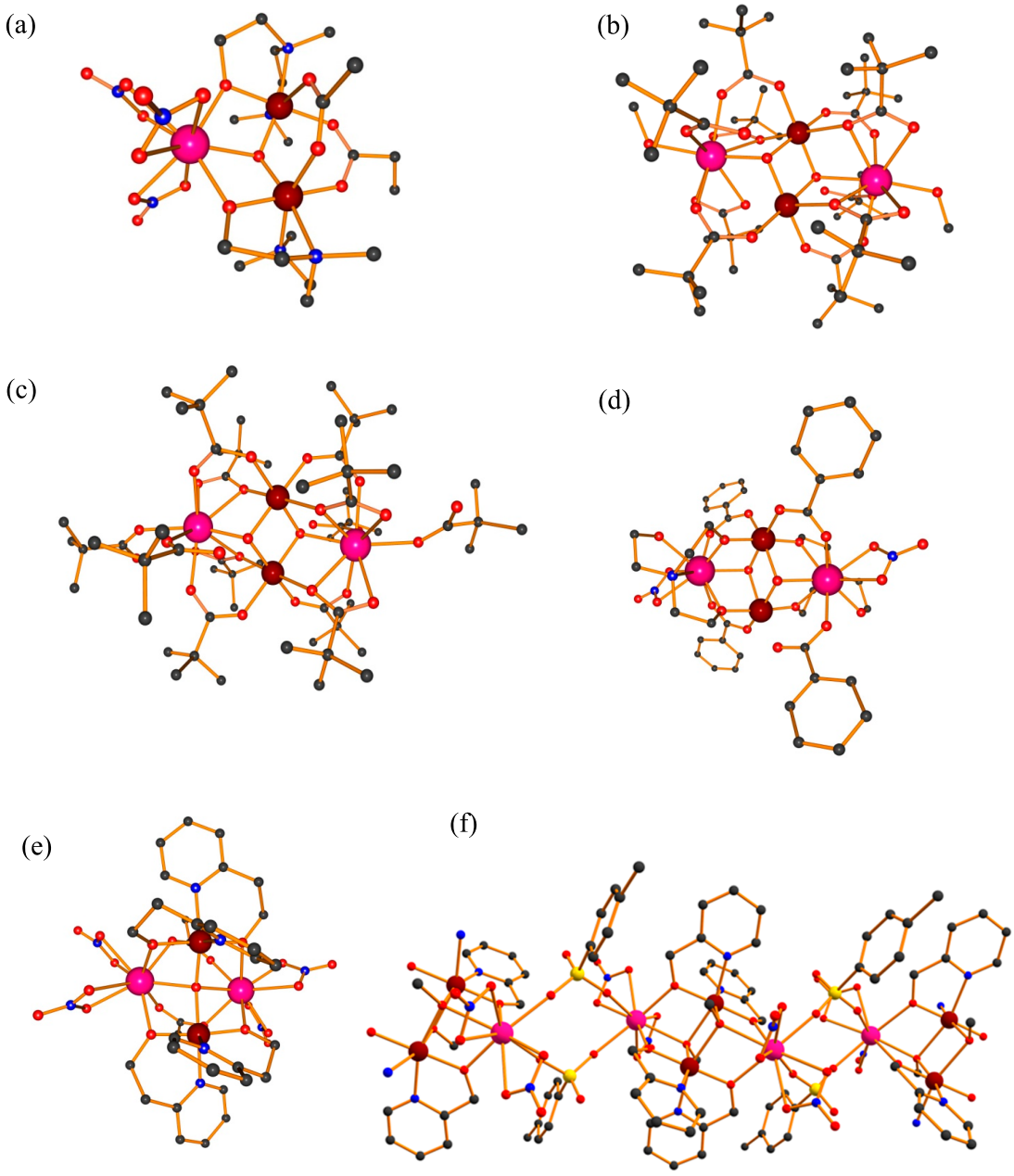

Figure 1. Molecular structures of **1** (a), **2** (b), **3** (c), **4** (d), **5** (e), and **6** (f) Color codes: pink, Gd; maroon, Mn; red, O; blue, N; gray, C; yellow, S. H atoms are omitted for clarity.

The largest number of unpaired electrons in f orbitals and the isotropic nature of Gd^{III} ion keep it as an attractive candidate for the application of magnetic refrigeration, and this can also be evidenced from the significant change in entropy values (ΔS_m) reported for several Gd^{III}-based complexes.[5−17] Another reason for the preference for the Gd^{III} ion in this area is its ability to promote weak exchange interaction due to the contracted nature of 4f orbitals; however, the nature of Gd^{III}−Gd^{III} coupling is difficult to control and has been found to be antiferromagnetic in many Gd^{III} complexes reported.[11,17−19] The nature of the coupling between Gd^{III} and 3d metal ions, on the other hand, is predictable, as they are generally ferromagnetic in nature with a few exceptions.[20−24] For this reason, several 3d Gd^{III} complexes have been targeted toward achieving large MCE values, and this approach has been very successful.[14,25−31] Among 3d ions, $Mn^{II/III}$ possesses a large number of unpaired electrons and is an ideal candidate, where the Mn^{II} ion is isotropic in nature while Mn^{III} possesses a significant single-ion zero-field splitting parameter. For this reason, Mn^{II} ions are preferred; however, Mn^{II} ions undergo facile oxidation and are hard to isolate, as evidenced by only a few reports on Mn^{II}−Gd^{III} complexes.[32−36] On the other hand, complexes containing Mn^{III} and Gd^{III} ions are the most common[27,31,37−52] and {Mn^{III}−Gd^{III}} interactions are generally ferromagnetic, and the only hurdle in realizing a considerable MCE value with this combination is the significant single-ion anisotropy of the Mn^{III} ions. One way to overcome this issue is by incorporating more than one Mn^{III} ion in the cluster aggregation so that the individual anisotropy of the Mn^{III} ions possibly cancel each other out, leading to large MCE values. While Mn^{III} clusters with very small and negligible anisotropy due to such cancellation are known,[53]

DOI: 10.1021/acs.inorgchem.9b01503
Inorg. Chem. 2019, 58, 11927−11940

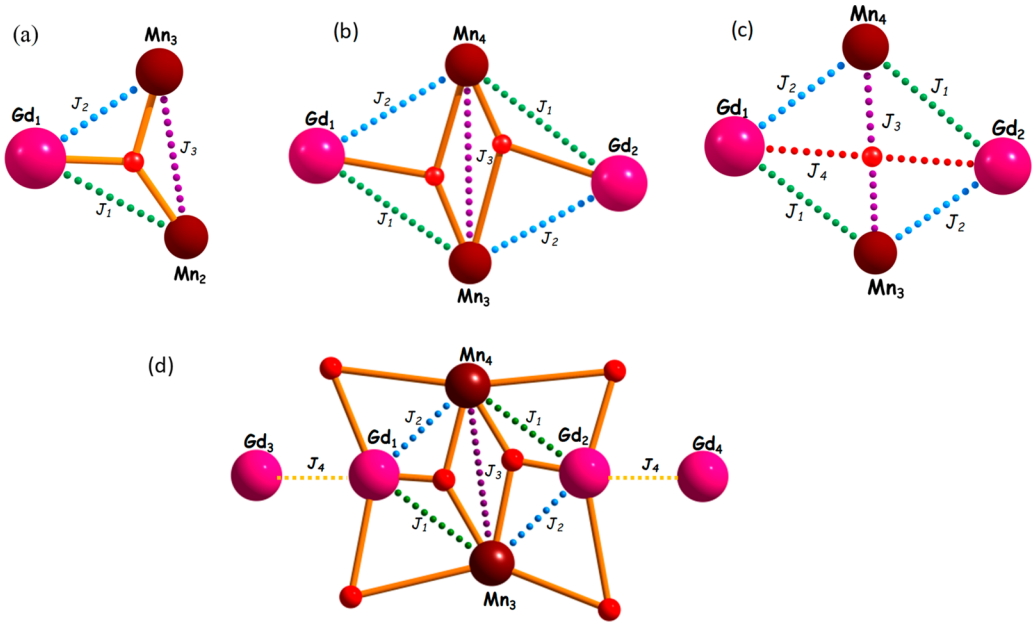

Figure 2. Exchange pathways in **1** (a), **2**–**4** (b), **5** (c), and **6** (d) (J_1 and J_2, {Mn^{III}–Gd^{III}}; J_3, {Mn^{III}–Mn^{III}}; J_4, {Gd^{III}–Gd^{III}}).

Table 1. DFT Computed and Experimentally Estimated *J* Values for 1–6[a]

	exchange interaction value (cm^{-1})				
	{Mn–Gd}				
complex	J_1	J_2	{Mn–Mn} J_3	{Gd–Gd} J_4	$J_1/\|J_3\|$
1	0.26	0.36	−7.55		0.03
2	0.54 (2.44)[41]	0.77 (2.44)	−69.55 (−62.91)	−0.002 (−0.01)	0.008
3	0.76	0.65	−70.11	0.0	0.011
4	−0.25	−0.19	−0.28	−0.001	0.89
5	0.03	−1.06	−13.94	0.05	0.002
6	−0.44 (−0.08)[65]	0.067(−0.08)	−1.64 (2.80)	−0.002	0.27

[a]Experimental *J* values are given in parentheses.

exploiting this very phenomenon to construct clusters possessing large MCE values has not been explored in detail.

Apart from ground-state and anisotropy values, the exchange value (J) is also an important parameter, as it will provide clues about the nature of the ground state and the ground-state–excited-state gap. The J values obtained by fitting the featureless $\chi_M T$ curves are often not reliable, and in this aspect, theoretical calculations[23,24,54−62] based on density functional methods have a proven track record to yield good numerical estimate of J values for 3d–Gd^{III} pairs. In addition, they also offer clues about the mechanism of magnetic coupling to gain insight into the sign and strength of computed J values.

Although the magnetic coupling has been explored in detail for several 3d–Gd pairs, there have only been a few studies on the magnetic coupling in Mn^{III}–Gd^{III} pairs.[24,63] Earlier, we studied numerous {Mn^{III}_2} dimers and proposed a classification based on the orientation of the Jahn–Teller axis, which not only controls the sign and strength of J values but is also correlated to the anisotropy.[64] Keeping this in mind, here we have studied a series polynuclear Mn^{III}–Gd^{III} complexes with an aim to answer the following intriguing questions. (i) How good are the DFT-computed J values in these types of clusters? (ii) What is the mechanism of magnetic coupling and how do the Mn^{III}–Gd^{III} and Mn^{III}–Mn^{III} interactions evolve with various structure topologies? (iii) How do structural topology and J values influence the MCE values? To answer these intriguing questions, we have chosen a series of Mn^{III}–Gd^{III} clusters containing a trinuclear complex {$Mn^{III}_2Gd^{III}$}, $[Mn_2GdO(Piv)_2(dmem)_2(NO_3)_3]$ (**1**),[51] along with four other tetranuclear complexes {$Mn^{III}_2Gd^{III}_2$}, $[Mn_2Gd_2O_2(Piv)_8(HO_2CCMe_3)_2(MeOH)_2]$ (**2**),[41] $[Mn_2Gd_2O_2(Piv)_8(HO_2CCMe_3)_4]$ (**3**),[51] $[Mn_2Gd_2(OH)_2(O_2CPh)_4(NO_3)_2(teaH)_2]$ (**4**),[51] and $[Mn_2Gd_2(O)(Piv)_2(hep)_4(NO_3)_4]$ (**5**),[49] and a single-chain compound containing the {$Mn^{III}_2Gd^{III}_2$} core, $[Mn_2Ln_2(OH)(OMe)(hmp)_4(NO_3)_4(O_3SC_6H_4CH_3)_2]_n$ (**6**),[65] for our calculations. The X-ray structures of these complexes are shown in Figure 1.

COMPUTATIONAL METHODOLOGY

The different exchange pathways modeled in trinuclear (**1**) and tetranuclear complexes (**2**–**6**) are shown in Figure 2. To extract J values in tetranuclear complexes, Noodleman's[66] broken symmetry method is employed. The different spin state configurations (one high spin and four broken symmetry solutions) are used to extract J values, are shown in Table 1.

The different Hamiltonian equations employed to extract J values for complex **1** (eq 1), complexes **2**–**5** (eq 2), and complex **6** (eq 3) are shown below.

$$\hat{H}_{Ex} = -[J_1(\hat{S}_{Gd1}\hat{S}_{Mn2}) + J_2(\hat{S}_{Gd1}\hat{S}_{Mn3}) + J_3(\hat{S}_{Mn2}\hat{S}_{Mn3})] \quad (1)$$

DOI: 10.1021/acs.inorgchem.9b01503
Inorg. Chem. 2019, 58, 11927−11940

$$\hat{H}_{Ex} = -[J_1(\hat{S}_{Gd1}\hat{S}_{Mn3} + \hat{S}_{Gd2}\hat{S}_{Mn4}) + J_2(\hat{S}_{Gd1}\hat{S}_{Mn4} + \hat{S}_{Gd2}\hat{S}_{Mn3}) + J_3(\hat{S}_{Mn3}\hat{S}_{Mn4}) + J_4(\hat{S}_{Gd1}\hat{S}_{Gd2})] \quad (2)$$

$$\hat{H}_{Ex} = -[J_1(\hat{S}_{Gd1}\hat{S}_{Mn3} + \hat{S}_{Gd2}\hat{S}_{Mn4}) + J_2(\hat{S}_{Gd1}\hat{S}_{Mn4} + \hat{S}_{Gd2}\hat{S}_{Mn3}) + J_3(\hat{S}_{Mn3}\hat{S}_{Mn4}) + J_4(\hat{S}_{Gd3}\hat{S}_{Gd1} + \hat{S}_{Gd2}\hat{S}_{Gd4})] \quad (3)$$

All the calculations were performed using the Gaussian 09[67] suite of programs with a combination of a hybrid UB3LYP[68] (unrestricted Becke-style three-parameter DFT using the Lee−Yang−Parr correlation) functional. The basis set employed for different elements are as follows: TZV[69] for Mn^{III} ions, SVP[69] for C, N, and O; SV for H and with a double-ζ quality basis set employing a Cundari−Stevens relativistic effective core potential (ECP)[70] (named CSDZ) on the Gd^{III} ion. In the ECP treatment, the core electrons are modeled using a suitable function and only the valence electrons are treated explicitly. The relativistic effects are vital for the rare-earth ions, and here they are incorporated by employing a relativistically corrected ECP basis set; this is found to yield a good numerical estimate of J values for several di- and polynuclear clusters.[23,24,54−62] The simulation of magnetic susceptibility data and eigenvalue plots were obtained using MAGPACK software.[71] The ΔS_m values were computed using PHI software.[72] To estimate the errors in the computed J values, we have utilized the energies computed in complex **1** and assumed $J_1 \approx J_2$ scenario; this yields $J_1 = 0.19$ cm^{-1} and $J_3 = -7.27$ cm^{-1}, on which the calculated errors are 0.028 cm^{-1} on J_1 and 0.29 cm^{-1} on J_3 offering confidence in the sign and strength of estimated J values.

RESULTS AND DISCUSSION

Complex **1**, $\{Mn_2Gd\}$, is a trinuclear complex consisting of a Gd^{III} ion and two Mn^{III} ions arranged in a triangular fashion (see Figure 1). The tetranuclear $\{Mn^{III}_2Gd^{III}_2\}$ complexes **2**−**5** consist of two Mn^{III} ions and two Gd^{III} ions in which complexes **2**−**4** possess similar topologies, commonly termed a distorted-butterfly structure, whereas complex **5** has a square geometry. The Mn^{III} ions are found to be six-coordinated in a distorted-octahedral environment, and the Gd^{III} ions possess nine-coordination with a distorted-square-antiprismatic geometry. Complex **6** is a one-dimensional coordination polymer consisting of a tetranuclear array of two Mn^{III} ions and two Gd^{III} ions possessing a butterfly structure similar to that of complexes **2**−**4** (see Figure 1). In the next sections, we will be discussing the exchange pathways individually along with their mechanism of magnetic coupling. Computed J values for complexes **1**−**6** are shown in Table 1, and the corresponding structural parameters that are expected to influence these J values are given in Table 2. The computed values are in good agreement with the experimental J values reported for complex **2**, though the experimental fits did not include the single-ion zero-field splitting of Mn(III) ions.[41] As the experimental J values are not available for other structures, we have simulated the susceptibility data using DFT-computed J values for complexes **1**−**6**, and this offers a good fit to the experimental susceptibility data and offers confidence in the estimated J values (see Figure S1 in the Supporting Information). In the next section, we discuss in detail the individual exchange coupling estimated across complexes **1**−**6** before turning to assess the role of J values in the estimation of the MCE values.

Table 2. Structural Data Corresponding to {Mn−Gd} Exchange Interactions for Complexes 1−6

exchange interaction	bond distance Mn−O (Å)	bond distance Gd−O (Å)	bond angle Mn−O−Gd (deg)	dihedral angle Mn−O−Gd−O (deg)
1				
J_1	1.90, 1.84	2.38, 2.35	102.3, 105.5	10.1
J_2	1.92, 1.84	2.33, 2.35	102.7, 104.8	9.6
2				
J_1	1.91, 2.30	2.38, 2.49	107.8, 92.7	16
	1.90, 2.30	2.38, 2.49	107.8, 92.7	15.6
J_2	1.88, 2.23	2.38, 2.54	108.4, 93.1	16.3
	1.88, 2.23	2.38, 2.54	108.4, 93.1	16.3
3				
J_1	1.90, 2.27	2.35, 2.52	108.8, 92.6	16.2
	1.90, 2.27	2.35, 2.52	108.8, 92.6	16.2
J_2	1.90, 2.19	2.35, 2.51	107.2, 93.4	16.2
	1.90, 2.19	2.35, 2.51	107.2, 93.4	16.2
4				
J_1	1.97, 1.89	2.37, 2.33	101.7, 106.1	8.1
	1.97, 1.88	2.37, 2.33	101.7, 106.1	8.1
J_2	2.21, 1.90	2.37, 2.40	97.7, 106.3	7
	2.21, 1.90	2.37, 2.40	97.7, 106.3	7
5				
J_1	1.92, 1.87	2.42, 2.40	101.6, 104.0	9.9
	1.90, 1.87	2.46, 2.41	101.6, 104.3	9.2
J_2	1.92, 1.87	2.46, 2.34	92.3, 97.3	29.2
	1.90, 1.88	2.42, 2.36	94.0, 96.2	28.1
6				
J_1	1.89, 2.07	2.48, 2.38	108.8, 99.3	0.07
	1.89, 2.07	2.48, 2.38	108.8, 99.3	0.06
J_2	1.91, 2.30	2.48, 2.37	112.5, 96.4	1.45
	1.91, 2.30	2.48, 2.37	112.5, 96.4	1.13

Mn^{III}−Gd^{III} Exchange (J_1 and J_2 Interactions). The exchange interaction between Mn^{III} and Gd^{III} is found to be mediated via different bridging modes: case a, in complex **1** via μ_3-O(oxo) and μ_2-O(ligand); case b, in complexes **2**−**4** via μ_3-O(oxo) (μ_3-O(H) in the case of **4**) and the pivalate groups in two different bridging modes, η^1:η^1 and η^1:η^2; case c, via μ_3-O(oxo) and μ_2-O(ligand) for J_1 and via μ_3- O(oxo), μ_2-O(ligand), and a pivalate group in an η^2:η^1 fashion for the J_2 interaction in complex **5**; case d, via μ_4-O(Me) and μ_3-O (ligand) for J_1 and J_2 interactions for complex **6** (see Figure 1). Note here that, for complexes **1**−**4** and **6**, the J_1 and J_2 exchange topologies are the same while the structural parameters which control the J values are slightly different. In complex **5**, the exchange topologies for J_1 and J_2 are different. From Table 1, the following points emerge. (i) The magnitudes of the J values are found to be small in all cases. (ii) The Mn^{III}−Gd^{III} interaction is found to be ferromagnetic in complexes **1**−**3** while it is found to be antiferromagnetic in **4**. Complexes **5** and **6** found to possess antiferromagnetic J values with no or extremely weak ferromagnetic coupling. The magnitude of the ferromagnetic J values was found to vary from 0.03 to 0.77 cm^{-1}, and this is strongly correlated to the Mn−O−Gd angle (see Table 2), with larger angles favoring ferromagnetic coupling. The smaller Mn−O−Gd angles as low as 92.3° observed for complex **5** lead to a strong antiferromagnetic J_2 interaction. (iii) While the $J_1 \approx J_2$ scenario is noted for complexes **1**−**4**, for complexes **5** and **6** the values

DOI: 10.1021/acs.inorgchem.9b01503
Inorg. Chem. 2019, 58, 11927−11940

Scheme 1. Qualitative Mechanism of Magnetic Coupling Operational in the $\{Mn_2Gd_2\}$ System Studied

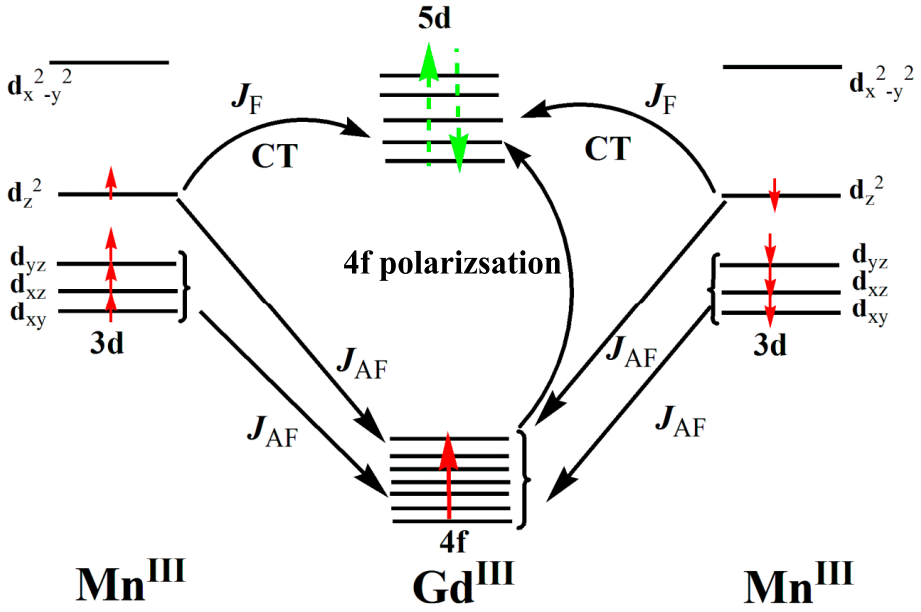

are drastically different. For complex **5** this is mainly due to the fact that the Mn−O−Gd angles associated with J_1 interactions are relatively large (the average angle is 102.8°), while the angles corresponding to J_2 are smaller (average angle is 95.0°). In addition, the Mn−O−Gd−O dihedral angles are also drastically different here with 9.5° noted for the J_1 interaction and 28.6° noted for the J_2 interaction. Both smaller Mn−O−Gd angles and larger dihedral angles observed for the J_2 interaction favor strong antiferromagnetic coupling, and the absence of this leads to weak ferromagnetic coupling for J_1. (iv) The J_1 and J_2 interactions in **4** are both antiferromagnetic due to smaller Mn−O−Gd angles. In addition to this effect, the Mn−O distances are important, as Mn−O distances as short as 1.88 Å and as long as 2.30 Å are observed. For the J_1 interactions in **4**, all of the Mn−O distances are short, as the Jahn−Teller axis does not pass through these oxygen atoms, while for J_2 the Mn−O distances are longer. For complex **6**, J_1 is found to be antiferromagnetic while J_2 is relatively weak and ferromagnetic in nature. Here the average Mn−O−Gd angles are found to be very similar (∼104°); however, the J_2 interaction is mediated via the Jahn−Teller elongated axis of the Mn^{III} ions, as reflected in longer Mn−O distances, and is likely to contribute significantly to the ferromagnetic coupling (see below), leading to the observed variation in the J values. Despite the fact that the $J_1 \approx J_2$ scenario is assumed in the experimental fittings, the sign coupling is reproduced in our calculations but the magnitudes of J values are underestimated.[65]

Mechanism of Magnetic Coupling in the {Mn−Gd} Pair. To understand the ferro−antiferro J values observed for the {Mn−Gd} pair, we have probed the mechanism of magnetic coupling using molecular orbital (MO) and natural bond orbital (NBO) analysis. In our earlier studies on other 3d−4f clusters,[73−75] we have proposed a generic mechanism for the exchange coupling, which shows the existence of two contributions (J_F and J_{AF}) to the overall exchange parameter. The contribution for the J_{AF} arises from the overlap between nonorthogonal d orbitals of Mn^{III} ions and the 4f orbitals of Gd^{III} ions. Orthogonality between the 3d and the 4f SOMOs contributes to the J_F term along with charge transfer from the 3d metal orbitals to the formally empty 5d orbitals of the Gd^{III} ions. These empty 5d orbitals play a proactive role in controlling the sign and strength of the magnetic coupling. The dominant factor between J_F and J_{AF} will decide the sign of the overall exchange. The overlap integrals between the SOMOs of 3d ions and Gd^{III} ions offer insight into the J_{AF} contribution, while the NBO calculations provide insight into the 5d orbital occupation. A schematic mechanism developed for $\{Mn_2Gd\}$ pair is shown in Scheme 1. As the $Mn^{III}\cdots Mn^{III}$ interactions are antiferromagnetic in all of the complexes, spin-up in one Mn^{III} center and spin-down in another Mn^{III} center are assumed.

The unpaired electron in the $3d_{z^2}$ orbital of the Mn^{III} ion is likely to play an active role both in contributing to the J_F term via charge transfer and to the J_{AF} term via overlap with 4f orbitals of Gd^{III} ion (σ-type orbital). The following points emerge from the mechanism developed. (i) The weak ferromagnetic {Mn−Gd} coupling observed in complex **1** is correlated to the dominant J_F term. The dominant J_{AF} term arises from the overlap of $3d_{z^2}$ with a $4f_{z^3}$ orbital of the Gd^{III} ion (see Figure 3). However, as the J-T axis of the Mn^{III} ion is parallel to the $\{MnGdO_2\}$ plane, this leads to less efficient overlap and hence a dominating ferromagnetic coupling. (ii) For complexes **2** and **3** as well, the J-T axes are perpendicular to the $\{MnGdO_2\}$ plane, ensuring weaker overlap. In fact, f_{z^3}−d_{xz}/d_{yz} was found to overlap significantly in these complexes, leading to a dominant J_{AF} contribution from this pair (se Tables S1 and S2 in the Supporting Information). As charge-transfer contribution is significant and dominating (Scheme 1), this leads to weak ferromagnetic $\{MnGd_4\}$ coupling for these complexes. (iii) For complex **4**, the J-T axes of the Mn^{III} ion are passing via the Mn−O−Gd axis, and this leads to dominant overlap with the $3d_{z^2}$ orbital of the Mn^{III} ion with several 4f orbitals of the Gd^{III} ion (See Figure 3). In addition to the $3d_{z^2}$ orbital, the $3d_{xy}$ and $3d_{xz}$ orbitals also overlap significantly with the 4f orbitals. This suggests dominant J_{AF} contributions, leading to antiferromagnetic coupling. (iv) In complex **5**, the J-T. axes are perpendicular to the $\{MnGdO_2\}$ plane; however,

DOI: 10.1021/acs.inorgchem.9b01503
Inorg. Chem. 2019, 58, 11927−11940

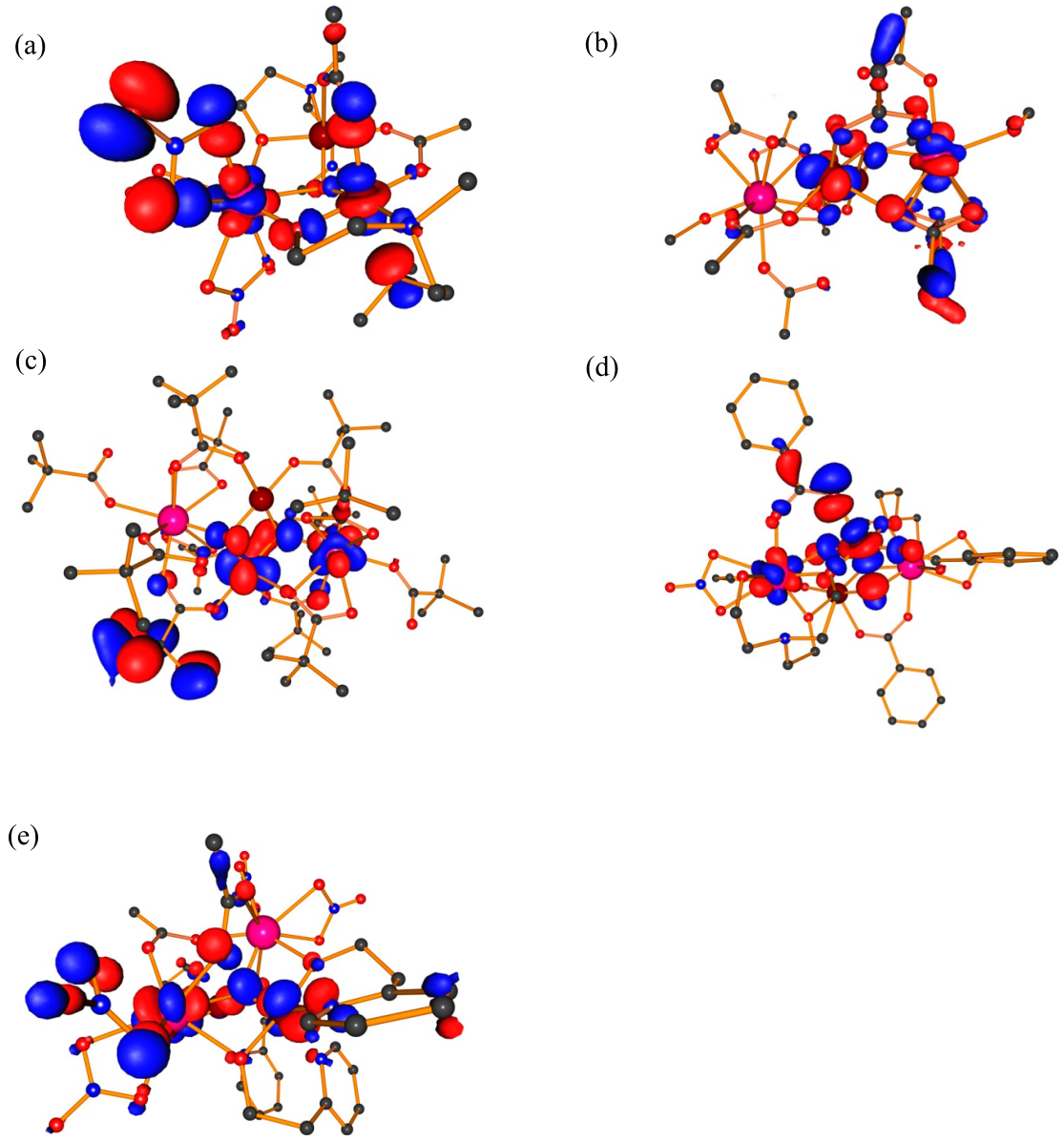

Figure 3. Representative orbitals for the maximum overlap observed (see Tables S2−S6 in the Supporting Information for computed overlap integral values) between the d orbitals of Mn^{III} ion and 4f orbitals of Gd^{III} ion for **1** (a), **2** (b), **3** (c), **4** (d), and **5** (e).

the Mn−O−Gd angle plays a role in controlling both the J_F and J_{AF} parameters. For the J_1 interaction where the Mn−O−Gd angle is larger, the charge-transfer contribution is significant, leading to dominant J_F contributions. At the same time, there are also some dominant 3d−4f overlaps (see Table S3 in the Supporting Information), leading to larger J_{AF} terms. This leads to a net cancellation and uncoupled {MnGd} situation. For J_2 interactions, on the other hand, the Mn−O−Gd angles are smaller, and this restricts CT contributions and hence the J_F term. In addition, several dominant overlaps of 4f orbitals with the multiple 3d orbitals are detected, suggesting dominant contributions from the J_{AF} term (see Figure 3). As the former is small/negligible while the latter is dominating, this leads to a strong antiferromagnetic J_2 interaction for complex **5**. (v) In complex **6** the average Mn−O−Gd angles are very similar and so are the Mn−O−Gd−O dihedral angles; however, the J_2 interaction lies along the direction of J-T axes and hence is expected to have dominant J_F contribution leading to extremely weak ferromagnetic coupling. For the J_1 interaction, the J_F term is expected to be small, leading to a dominant J_{AF} term as dictated by the angle.

Mn^{III}−Mn^{III} Interaction (J_3 Interaction). The exchange interaction between Mn^{III} ions are mediated via μ_3-O(oxo) and two pivalate groups in an η^1:η^1 bridging mode for complex **1**, via two μ_3-O(oxo) bridges for complexes **2**, **3**, and **6** (μ_3-O(H) for complex **4**), and via μ_4-O(oxo) for complex **5**. In all of the complexes, the J_3 interaction is found to be antiferromagnetic; however, the strength of J differs drastically, as shown in Table 1. The Mn^{III}−Mn^{III} exchange interaction in complexes **2** and **3** is found to be strongly antiferromagnetic in nature, followed by a moderate exchange in the case of complexes **1**, **5**, and **6** and weak antiferromagnetic exchange for complex **4**. While the J_3 values estimated for complex **2** are in agreement with experiments, for complex **6** the sign of J values obtained from experimental fitting is ferromagnetic, while our calculations suggest it to be antiferromagnetic. However, a good fit to the susceptibility data obtained from the DFT-estimated J values offers confidence in the computed J values.

DOI: 10.1021/acs.inorgchem.9b01503
Inorg. Chem. 2019, 58, 11927−11940

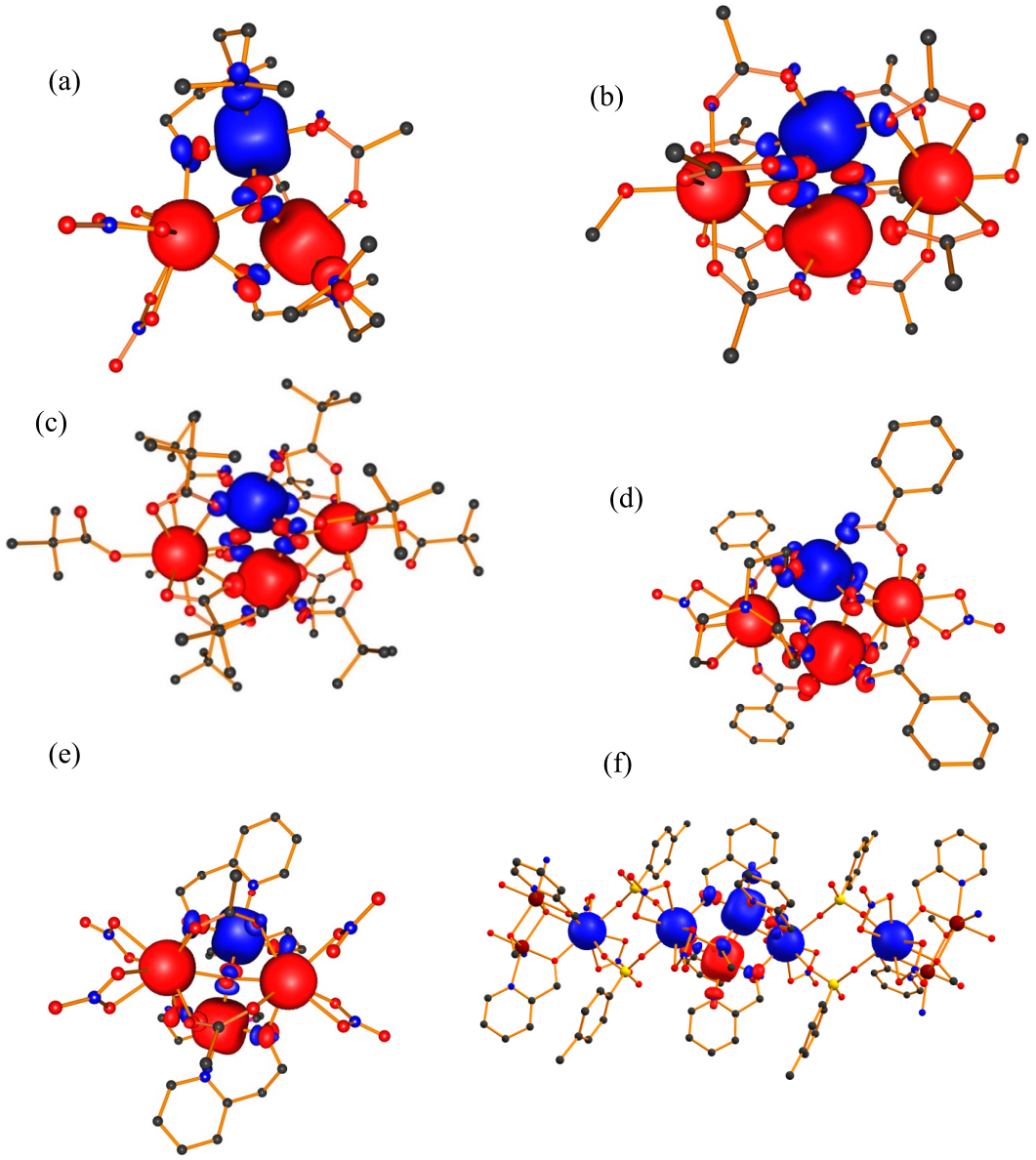

Figure 4. DFT-computed spin density for one of the broken-symmetry solution computed for **1** (a), **2** (b), **3** (c), **4** (d), **5** (e), and **6** (f).

Selected structural parameters that control the J_3 interactions are summarized in Table S4 in the Supporting Information.

In our previous study,[64] we found that the dihedral angle between J-T axes in $\{Mn^{III}_2(OR)_2\}$ is the prominent parameter in controlling the sign and magnitude of exchange. The $\{Mn^{III}_2(OR)_2\}$ core in complexes **2**–**4** has a topology similar to that of the systems studied earlier. As per our earlier definition, complexes **2** and **3** belong to type I, while complex **4** belongs to type II (see Scheme 1 for the orbital orientation observed). As the J-T axes of the Mn^{III} ions are found to lie parallel to each other but perpendicular to the Mn−O−Mn−O plane in complexes **2** and **3**, the dominant cross-interaction between the SOMO of the d_{z^2} to the empty $d_{x^2-y^2}$ orbital is very weak, leading to small or negligible contributions to the ferromagnetic part of the exchange. In addition, the Mn−O−Mn angles are relatively smaller (~98°) in comparison to those in the dinuclear $\{Mn^{III}_2(OR)_2\}$ complexes studied and this also enforces dominant overlaps among the t_{2g} orbitals (see Tables S1 and S2 in the Supporting Information for computed overlap integrals), leading to a significant contribution to the antiferromagnetic part of the exchange. As the J_{AF} term is dominating, this leads to a strong net antiferromagnetic J for complexes **2** and **3**. For complexes **4** and **6**, on the other hand, J-T axes are along the Mn−O−Mn−O axis, which results in significant $|d_{z^2}-d_{x^2-y^2}|$ cross-interaction, leading to a larger J_F term. Here also there are significant $|d_{xz}-d_{yz}|$, $|d_{xy}-d_{xz}|$, $|d_{yz}-d_{yz}|$ and $|d_{xy}-d_{yz}|$ overlaps; however, the $|d_{xy}-d_{xy}|$ overlap is relatively weaker in comparison to those in **2** and **3** due to the longer $Mn^{III}\cdots Mn^{III}$ distances observed in **4**. Due to competing ferro- and antiferromagnetic contributions, the net J noted here is small, albeit it is antiferromagnetic.

Complexes **1** and **5** also exhibit weak antiferromagnetic coupling, and in both cases, the exchange is mediated via one μ-oxo bridge. For both complexes **1** and **5** moderate overlaps among the t_{2g} orbital with weaker cross-interaction is expected. However, here the Mn−O−Mn angles are relatively large (120.5° for complex **1** and 144.8° for complex **5**), and this larger angle leads to competing antiferro−ferro terms leading to moderate antiferromagnetic coupling (see the Supporting Information for computed overlap integrals).

DOI: 10.1021/acs.inorgchem.9b01503
Inorg. Chem. 2019, 58, 11927−11940

Gd^{III}–Gd^{III} Interaction (J_4 Interaction). This additional interaction has been considered only in the case of complex **6**, where due to its one-dimensional chainlike structure the $Gd^{III}\cdots Gd^{III}$ interaction between two $\{Mn_2Gd_2\}$ units is envisioned. DFT calculations predict the existence of very weak exchange between Gd^{III} ions due to the contracted nature of 4f ions. The {Gd–Gd} interaction is a next-nearest-neighbor (1,3) interaction in complexes **2** and **4**, whereas it is a (1,2) interaction (bridged via oxo group and two carboxylate bridges) in complex **5**. This interaction is found to be antiferromagnetic in complexes **2**, **4**, and **6** while it is found to be weakly ferromagnetic in complex **5**. MO analysis shows the existence of a very weak overlap between 4f orbitals along with charge transfer to empty 5d/6s/6p, leading to a weak ferromagnetic interaction in complex **5**. The ferromagnetic coupling may also be attributed to large Gd–O–Gd angles (129.8°).[59] It is important to note here that, in complex **6**, the interaction is mediated via a benzenesulfonate ligand, which is very similar to the carboxylate bridge and offers only a very weak exchange between two Gd^{III} ions and hence the magnetic properties of this cluster are expected to be similar to those of the stand-alone $\{Mn_2Gd_2\}$ cluster.

Ground State and Spin Density Analysis of Complexes 1–6. To gain an understanding of the nature of the ground state manifested by the exchange interaction computed, we have analyzed the energy levels along with the spin density of the complexes **1**–**6**. The computed spin density plots for complexes **1**–**5** is shown in Figure 4 (See Figure S2 in the Supporting Information for complex **6**) The spin densities of Gd^{III} ions (~7.01) indicate the presence of spin polarization, as the 4f orbitals are deeply buried. In contrast, the spin density of Mn^{III} ions is ~3.8, which is lower than the spin density expected for four unpaired electrons. In the Mn^{III} ion the unpaired electrons reside in three t_{2g} orbitals and an e_g type d_{z^2} orbital. This promotes both polarization and delocalization mechanisms (along the Jahn–Teller elongated axis where d_{z^2} orbitals are located; see Figure 4). For complexes **1**–**3**, the μ_3-oxo bridge was found to possess a very small negative spin density (for the $S = 7/2$ state for **1** and $S = 7$ state for **2** and **3**); as this lies perpendicular to the Jahn–Teller axis, the Gd^{III} and Mn^{III} ions promote spin polarization. However, the effects of Mn^{III} ions are canceled as one possesses α-spin (spin-up) while the other possesses β-spin (spin-down) and the net effect visible is due to the polarization of Gd^{III}. Such a small polarization is correlated to the weaker {MnGd} coupling observed. For complexes **4** and **5**, on the other hand, the μ-oxo bridges were found to have positive spin densities. This is due to the fact that the Mn^{III} ion promotes dominant delocalization along these bridges and such a switch in the mechanism is found to yield antiferromagnetic {MnGd} coupling. This suggests that the spin density on the dominant exchange pathway could be used as a guideline to determine the sign of J in {MnGd} complexes.

The dominant antiferromagnetic interaction between two Mn^{III} ions in complex **1** results in the ground spin state of $S = 7/2$, and this is in accord with the experimental prediction. In the case of complexes **2**, **3**, and **5** the antiferromagnetic interaction between Mn^{III} ions leads to the competing interactions[76] within $\{Mn_2Gd\}$ triangles, resulting in the overall ground spin state being $S = 0$ (see Figure 4b,c,e). However, in complexes **2** and **3**, either the $J_3 \gg J_2 > J_1$ or $J_3 \gg J_1 > J_2$ situation arises, leading to an $S = 0$ spin ground state. To further understand how this ratio controls the ground state, we have created an Eigen plot of spin state energy against the ratio of $J_1/|J_3|$ (see Figure 5).

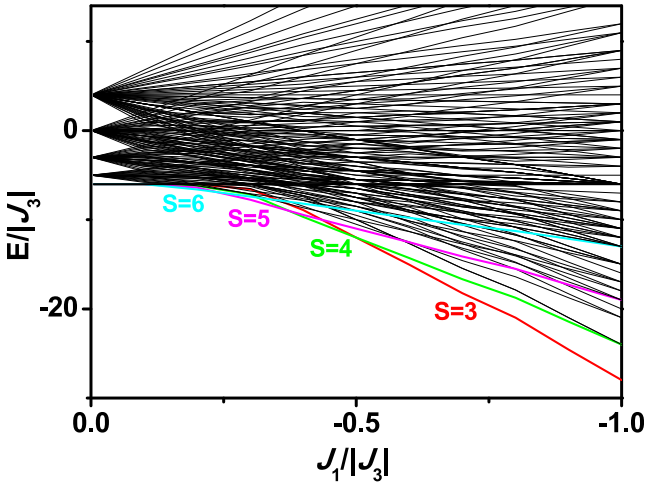

Figure 5. Plot of DFT calculated Eigen plots versus J_1/J_3 in complex **4**.

The variation in the ground-state values is correlated to the J_1/J_3 ratio. The plot clearly shows that ground state $S = 0$ becomes stabilized at a low J_1/J_3 ratio, which is reflected in the ground states of complexes **1**–**3** and **5**. However, in complex **4**, spin frustration and competing weak exchange interaction between different exchange pathways lead to a ground spin state of $S = 3$ (see Figure 4d). The J_1/J_3 ratio is −0.89, and the plots in the model complex (see Figure S3 in the Supporting Information for the structure of the model complex) shows that $S = 3$ is the ground state. For complex **6**, the ratio is small, and the J values are noncompeting, leading to an $S = 7$ ground state for the individual $\{Mn_2Gd_2\}$ units. Experimental fits suggest an $S = 3$ ground state with numerous other states lying just 1 cm^{-1} above the ground state. This suggests that the ground-state S values, as shown above, are very sensitive to even a small change in the J values. However, since the exchanges between $\{Mn_2Gd_2\}$ units are antiferromagnetic, this is likely to lead to an $S = 0$ ground state for the chain at extremely low temperatures. These results are in accord with the simulated susceptibilities and the experimental reports.

Magneto–Structural Correlations. To further elucidate the role of structural parameters that decides the strength and magnitude of {Mn–Gd} exchange, we have developed magneto–structural correlations by varying (a) Mn–O and Gd–O bond lengths, (b) Mn–O–Gd angles, and (c) Mn–O–Gd–O dihedral angles on a model complex (Figure S3 in the Supporting Information). The model complex (**1a**) has been designed out of complex **1**, and the {MnGd} exchange interaction is found to be ferromagnetic for this model (0.43 cm^{-1}).

Average Mn–O and Gd–O Distances. Magneto–structural correlations are performed by varying the Mn–O and Gd–O distances from 1.92 to 2.31 Å (the Mn–O distance is varied from 1.69 to 2.07 Å), and the fit to this correlation shows a parabolic trend (Figure 6a). The larger distances tend to favor moderately stronger ferromagnetic interaction, and this is because the larger angles lead to the weaker overlap of d_{xz}/d_{yz} with the 4f orbitals. More substantial overlaps of d_{xz}/d_{yz}, d_{z^2} orbitals with 4f orbitals in the intermediate bond distances tend to add strength to J_{AF} terms, leading to a smaller

DOI: 10.1021/acs.inorgchem.9b01503
Inorg. Chem. 2019, 58, 11927–11940

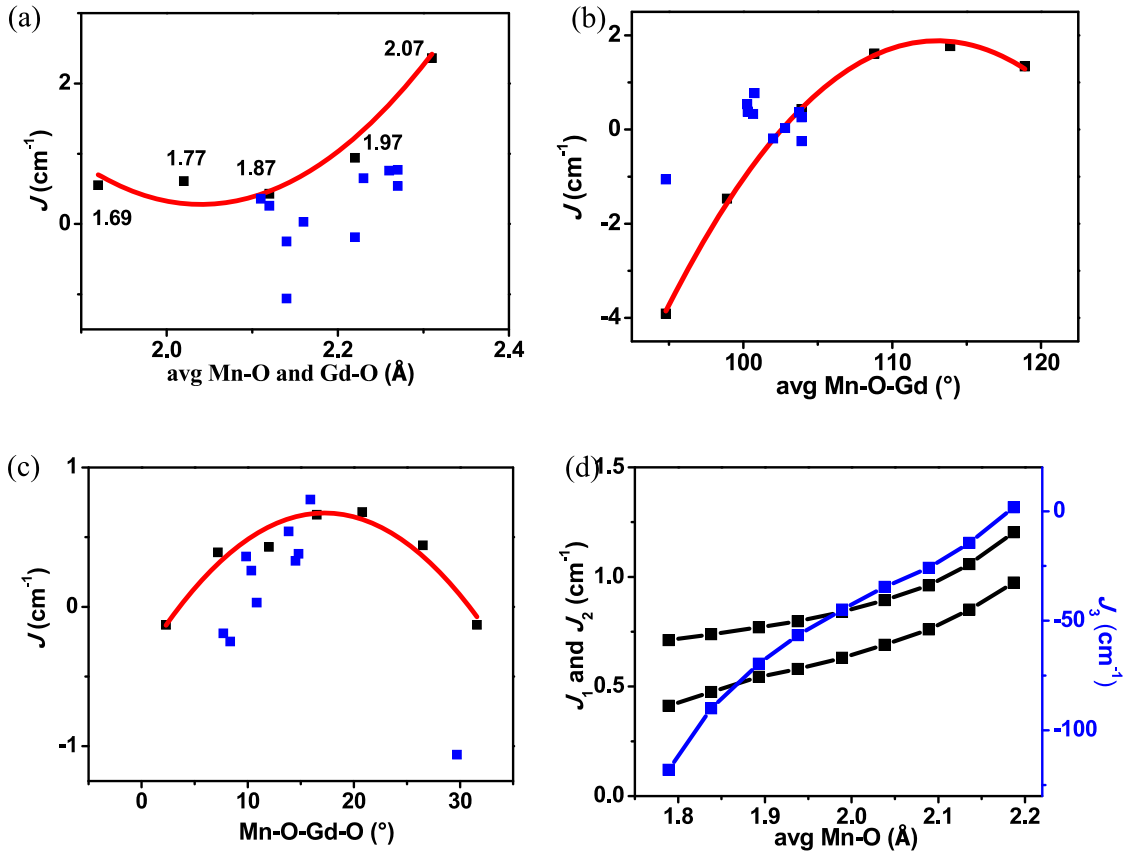

Figure 6. Developed magneto−structural correlations by varying (a) Mn−O and Gd−O bond distances, best fitting obtained with $y = a + bx + cx^2$ where $a = 122.46$, $b = -119.79$, and $c = 29.36$. (b) Mn−O−Gd angles, best fitting obtained with $y = a + bx + cx^2$, where $a = -218.90$, $b = 3.91$, and $c = -0.02$. (c) Mn−O−Gd−O dihedral angles in complex **1a**, best fitting obtained with $y = a + bx + cx^2$ where $a = -0.40$, $b = 0.12$, and $c = -0.004$. (d) Mn−O distances in complex **2**. Blue and black squares are the DFT-computed J values for complexes **1**−**5**.

ferromagnetic interaction (Table S5 in the Supporting Information). Upon variation of the bond lengths, the magnitude of exchange values tend to fluctuate but remains in the ferromagnetic zone. This shows that bond length is not a deciding factor in controlling the sign of J values.

Average Mn−O−Gd Angles. In the second correlation developed, we have varied the Mn−O−Gd angle from 94.8 to 118.9°, and the data fit into the parabolic curve (Figure 6b). Lower angles favor an antiferromagnetic interaction, whereas a larger angle favors a ferromagnetic interaction. At lower angles, the overlap between the f orbitals with d_{xy} and d_{xz}/d_{yz} are predominant (Table S6 in the Supporting Information), which considerably decreases upon an increase in the angles, resulting in dominant J_F and J_{AF} terms at larger angles and smaller angles, respectively. Apart from this, the smaller angles tend to diminish the channel for charge transfer, resulting in a dominant J_{AF} term and thus explaining the observed antiferromagnetic interaction at smaller angles. The Mn−O−Gd angle can switch the strength as well as the sign of the magnetic exchange interaction. A magneto−structural correlation for a $\{Mn^{III}Gd^{III}\}$ dinuclear complex was developed earlier, and these correlations are in line with those developed here.[31]

Average Mn−O−Gd−O Dihedral Angles. Apart from the distance and angle parameters, we have also developed a correlation by varying the Mn−O−Gd−O dihedral angles from 2.2° to 31.1°. A nonlinear curve fit to the developed correlation shows a parabolic fit in which smaller and larger dihedral angles favor weak antiferromagnetic interaction (see Figure 6c). The incorporation of experimental points shows scattered patterns with a better trend in the case of a dihedral correlation, and this parameter is also effective in controlling the sign (switches the sign of the exchange) of the exchange. The sign of the exchange is controlled by the overlap between the $d_{xz}/d_{zy}/d_{xy}$ orbitals and 4f orbitals (Table S7 in the Supporting Information) at smaller and larger angles, as evidenced in bond distance correlation. As a whole, both Mn−O−Gd angles and Mn−O−Gd−O dihedral angles play a vital role in deciding the sign and nature of the exchange interaction, in which smaller angles and larger dihedral angles lead to negative J values. This correlation proposed is consistent with earlier reports.[31]

We have also analyzed the effect of Mn−O distance on the Mn−Mn exchange, as this parameter is found to be an effective parameter in controlling the sign of exchange in $\{Mn^{III}{}_2(OR)_2\}$ complexes.[64] Here we have varied the average distance of Mn−O bond lengths from 1.79 to 2.19 Å, and their effects on the exchange values are shown in Figure 6d. The developed correlation indicates that the exchange becomes more strongly antiferromagnetic (−118.08 cm^{-1}) at smaller distances, whereas it is ferromagnetic (1.75 cm^{-1}) at larger distances. The effect of dihedral angles between J-T and Mn−O distance parameters on the exchange values validates our conclusions obtained from the simple dimeric $\{Mn^{III}{}_2(OR)_2\}$ units.[77]

Magnetocaloric Effect. After examining the exchange pathways, we have analyzed the MCE properties of complexes

DOI: 10.1021/acs.inorgchem.9b01503
Inorg. Chem. 2019, 58, 11927−11940

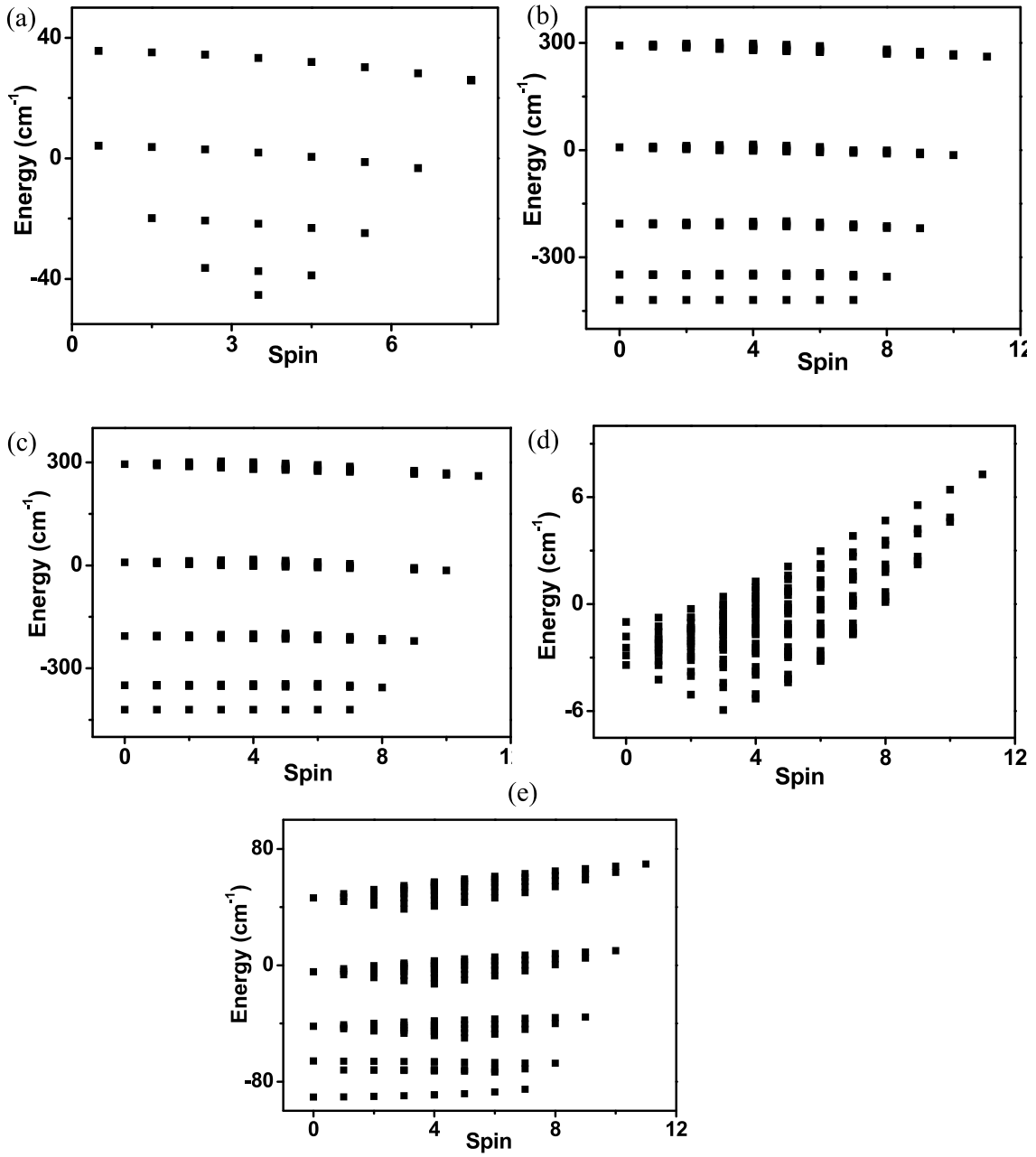

Figure 7. Eigen plot derived using DFT exchange parameters for complex **1** (a), complex **2** (b), complex **3** (c), complex **4** (d), and complex **5** (e).

1−**5** and excluded complex **6**, as it is one-dimensional chain and not a discrete molecule. Here, the changes in the entropy value have been calculated for complexes **1**−**5** using the Maxwell relations, $\Delta S_m(T)_{\Delta B} = \int\left[\frac{\partial M(T,B)}{\partial T}\right]_B dB$, and are found to be −13.5, −20.39, −19.73, −31.75, and −19.0 J/(kg K), respectively. The maximum attainable entropy changes for the uncoupled metal ion spins in complexes **1**−**5** are −45.79, −37.91, −36.64, −38.14, −44.48 J/(kg K) (3 K at 9 T). The magnitudes of the estimated ΔS_m values from the DFT-computed J values are comparatively smaller than the maximum attainable entropy values, with the exception of complex **4**, where the difference is relatively smaller. This can be attributed to the difference in the strength of J values and their molecular weights.

To probe this difference in ΔS_m values, energy level diagrams for complexes **1**−**5** are plotted (see Figure 7). From this plot, it is clear for all complexes except **4** that the energies of spin states are discrete with a significant gap among them. For complex **4**, on the other hand, the energy levels resemble that of a continuum with very close lying excited states. The scale of the y axis also sheds light on the energy splitting, where large energy gaps as much as 600 cm^{-1} are noted for complexes **2** and **3**, while for complex **4** all of the states lie within an energy span of 13 cm^{-1}. Very strong $Mn^{III}\cdots Mn^{III}$ exchange observed in complexes **2** and **3** and moderately large $Mn^{III}\cdots Mn^{III}$ exchange observed for complexes **1** and **5** are responsible for this gap. The large entropy change in the complex is mainly attributed to very close lying excited states, and this can be achieved if the exchange interaction is weak and competing or spin frustration results in degenerate states. In the case of complex **4**, competing exchange leads to spin frustration, leading to degenerate and close-lying states, and this results in appreciable ΔS_m values. The Mn^{III}−Mn^{III}

DOI: 10.1021/acs.inorgchem.9b01503
Inorg. Chem. 2019, 58, 11927−11940

exchange interaction are controlled by the nature of J−T axes (see in the Supporting Information). If the J-T axes of two Mn^{III} ions are perpendicular to each other, the exchange interaction will be moderately ferromagnetic in nature; a parallel orientation of J-T axes results in stronger antiferromagnetic interaction leading to lower ΔS_m values. This invariably suggests that a parallel orientation of J-T axes of Mn^{III} ion along the Gd−Mn−Mn−Gd plane is a preferable geometry to enhance the MCE values. The magnitude and sign of Mn−Gd exchange also be controlled by varying Mn−O−Gd−O dihedral angles and Mn−O−Gd angles. The better condition for magneto−caloric applications would be a weak exchange interaction, which can be obtained by suitable ligand design controlling these two structural parameters.

The parallel orientation of J-T axes of Mn^{III} ions in complex **1** would result in weaker J values in such instances, assuming the $\{Mn^{III}\cdots Gd^{III}\}$ exchange value would be -0.28 cm^{-1} (as observed in complex **4**) and the calculated $-\Delta S_m$ value is 37.9 J kg^{-1} K^{-1}. This invariably supports the need for low molecular weight to obtain larger MCE values, and thus fine-tuning of structural parameters regardless of the nature of magnetic anisotropy in low-nuclearity complexes would be the key to obtain robust MCE values.

CONCLUSIONS

In summary, we have performed a detailed DFT analysis on one trimeric, four tetrameric, and one 1D chain complex containing Mn^{III} and Gd^{III} ions, to understand the different exchange pathways and to probe the role of magnetic exchange in obtaining larger ΔS_m values in low nuclearity complexes.

Using DFT methodology, we obtain a good numerical estimate of J values, and the computed J values can reproduce the experimental data. The estimated J values show the existence of weak to strong antiferromagnetic exchange between Mn^{III} ions in these complexes, and this is correlated to the orientation of the J-T axis as predicted earlier. Our analysis shows that the charge transfer from Mn^{III} ion to the vacant 5d orbitals of Gd^{III} ion and the overlap between the SOMOs controls the sign of exchange interaction between Mn^{III} and Gd^{III} ions. We have developed magneto−structural correlations in a {MnGd} model which predict that the Mn−O−Gd−O dihedral angles and Mn−O−Gd angles hold the key in switching the sign of the exchange. This reiterates the need to understand the spin Hamiltonian parameters in simple building blocks before extending them to polynuclear complexes.

The existence of strong antiferromagnetic exchange between Mn^{III} ions induces competing interactions within the Mn_2Gd triangles of the tetranuclear complexes, resulting in an $S = 0$ ground spin state for complexes **2**, **3**, and **5**. However, the competing weak exchange interaction along with the presence of spin frustration effects results in an $S = 3$ ground state for complex **4** and $S = 7$ ground state for the $\{Mn_2Gd_2\}$ unit in complex **6**. In the case of complex **4**, weak exchange pulls the excited states much closer to the ground state, resulting in a large ΔS_m value like that in polynuclear clusters containing several metal ions. This suggests that invoking competing interactions/spin frustration on low-nuclearity complexes (trinuclear and tetranuclear) by ligand design can yield attractive ΔS_m values regardless of the nature of single-ion magnetic anisotropy. These suggestions are in line with earlier recommendations.[4] The search for other {3d−4f} nuclearity complexes that can offer such effects is underway in our laboratory.

ASSOCIATED CONTENT

Supporting Information

The Supporting Information is available free of charge on the ACS Publications website at DOI: 10.1021/acs.inorgchem.9b01503.

Simulated susceptibility plots for complexes **1**−**6**, computed overlap integrals, selected structural parameters that control the J values in complexes **1**−**6**, spin density plots for complex **6**, the model structure used for the developed correlation, and X-ray structures of complexes **1**−**6** showing the J-T axes (PDF)

AUTHOR INFORMATION

Corresponding Author

*G.P.: tel, (+91)-22-2576-7183; e-mail, rajaraman@chem.iitb.ac.in.

ORCID

Gopalan Rajaraman: 0000-0001-6133-3026

Notes

The authors declare no competing financial interest.

ACKNOWLEDGMENTS

G.R. thanks the UGC (UGC-UKIERI grant number 184-1/2018(IC)) and SERB (CRG/2018/000430) for funding. T.R. thanks IIT Bombay for the financial support (Research Associate fellowship). R.J. thanks DST-INSPIRE for a fellowship.

REFERENCES

(1) Feder, T. SLAC free-electron laser sparkles into life. *Phys. Today* **2009**, *62*, 21−22.

(2) Craig, G. A.; Murrie, M. 3d single-ion magnets. *Chem. Soc. Rev.* **2015**, *44*, 2135−2147.

(3) Gatteschi, D.; Sessoli, R.; Villain, J. *Molecular nanomagnets*; Oxford University Press: 2006; pp 1−10.

(4) Evangelisti, M.; Brechin, E. K. Recipes for enhanced molecular cooling. *Dalton Trans* **2010**, *39*, 4672−4676.

(5) Chen, Y. C.; Prokleska, J.; Xu, W. J.; Liu, J. L.; Liu, J.; Zhang, W. X.; Jia, J. H.; Sechovsky, V.; Tong, M. L. A brilliant cryogenic magnetic coolant: magnetic and magnetocaloric study of ferromagnetically coupled GdF3. *J. Mater. Chem. C* **2015**, *3*, 12206−12211.

(6) Hou, Y. L.; Xiong, G.; Shi, P. F.; Cheng, R. R.; Cui, J. Z.; Zhao, B. Unique (3,12)-connected coordination polymers displaying high stability, large magnetocaloric effect and slow magnetic relaxation. *Chem. Commun.* **2013**, *49*, 6066−6068.

(7) Han, S. D.; Miao, X. H.; Liu, S. J.; Bu, X. H. Magnetocaloric effect and slow magnetic relaxation in two dense (3,12)-connected lanthanide complexes. *Inorg. Chem. Front.* **2014**, *1*, 549−552.

(8) Xu, L. Y.; Zhao, J. P.; Liu, T.; Liu, F. C. Gadolinium Sulfate Modified by Formate To Obtain Optimized Magneto-Caloric Effect. *Inorg. Chem.* **2015**, *54*, 5249−5256.

(9) Han, S. D.; Miao, X. H.; Liu, S. J.; Bu, X. H. Large Magnetocaloric Effect in a Dense and Stable Inorganic-Organic Hybrid Cobridged by In Situ Generated Sulfate and Oxalate. *Chem. - Asian J.* **2014**, *9*, 3116−3120.

(10) Evangelisti, M.; Roubeau, O.; Palacios, E.; Camón, A.; Hooper, T. N.; Brechin, E. K.; Alonso, J. J. Cryogenic Magnetocaloric Effect in a Ferromagnetic Molecular Dimer. *Angew. Chem., Int. Ed.* **2011**, *50*, 6606−6609.

DOI: 10.1021/acs.inorgchem.9b01503
Inorg. Chem. 2019, 58, 11927−11940

(11) Guo, F.-S.; Leng, J.-D.; Liu, J.-L.; Meng, Z.-S.; Tong, M.-L. Polynuclear and Polymeric Gadolinium Acetate Derivatives with Large Magnetocaloric Effect. *Inorg. Chem.* **2012**, *51*, 405−413.
(12) Sharples, J. W.; Zheng, Y.-Z.; Tuna, F.; McInnes, E. J. L.; Collison, D. Lanthanide discs chill well and relax slowly. *Chem. Commun.* **2011**, *47*, 7650−7652.
(13) Chang, L.-X.; Xiong, G.; Wang, L.; Cheng, P.; Zhao, B. A 24-Gd nanocapsule with a large magnetocaloric effect. *Chem. Commun.* **2013**, *49*, 1055−1057.
(14) Hooper, T. N.; Inglis, R.; Palacios, M. A.; Nichol, G. S.; Pitak, M. B.; Coles, S. J.; Lorusso, G.; Evangelisti, M.; Brechin, E. K. CO2 as a reaction ingredient for the construction of metal cages: a carbonate-panelled [Gd6Cu3] tridiminished icosahedron. *Chem. Commun.* **2014**, *50*, 3498−3500.
(15) Jia, J.-M.; Liu, S.-J.; Cui, Y.; Han, S.-D.; Hu, T.-L.; Bu, X.-H. 3D GdIII Complex Containing Gd16 Macrocycles Exhibiting Large Magnetocaloric Effect. *Cryst. Growth Des.* **2013**, *13*, 4631−4634.
(16) Peng, J. B.; Kong, X. J.; Zhang, Q. C.; Orendac, M.; Prokleska, J.; Ren, Y. P.; Long, L. S.; Zheng, Z. P.; Zheng, L. S. Beauty, Symmetry, and Magnetocaloric Effect-Four-Shell Keplerates with 104 Lanthanide Atoms. *J. Am. Chem. Soc.* **2014**, *136*, 17938−17941.
(17) Roubeau, O.; Lorusso, G.; Teat, S. J.; Evangelisti, M. Cryogenic magneto-caloric effect and magneto-structural correlations in carboxylate-bridged Gd(III) compounds. *Dalton Trans* **2014**, *43*, 11502−11509.
(18) Anwar, M. U.; Dawe, L. N.; Tandon, S. S.; Bunge, S. D.; Thompson, L. K. Polynuclear lanthanide (Ln) complexes of a tri-functional hydrazone ligand - mononuclear (Dy), dinuclear (Yb, Tm), tetranuclear (Gd), and hexanuclear (Gd, Dy, Tb) examples. *Dalton Trans* **2013**, *42*, 7781−7794.
(19) Canadillas-Delgado, L.; Fabelo, O.; Pasan, J.; Delgado, F. S.; Lloret, F.; Julve, M.; Ruiz-Perez, C. Intramolecular ferro- and antiferromagnetic interactions in oxo-carboxylate bridged digadolinium(III) complexes. *Dalton Trans* **2010**, *39*, 7286−7293.
(20) Hooper, T. N.; Schnack, J.; Piligkos, S.; Evangelisti, M.; Brechin, E. K. The Importance of Being Exchanged: [GdIII4MII8-(OH)8(L)8(O2CR)8]4+ Clusters for Magnetic Refrigeration. *Angew. Chem., Int. Ed.* **2012**, *51*, 4633−4636.
(21) Georgopoulou, A. N.; Adam, R.; Raptopoulou, C. P.; Psycharis, V.; Ballesteros, R.; Abarca, B.; Boudalis, A. K. Isomorphous replacement of MII ions in MII-GdIII dimers (MII = CuII, MnII, NiII, CoII, ZnII): magnetic studies of the products. *Dalton Trans* **2010**, *39*, 5020.
(22) Costes, J.-P.; Garcia-Tojal, J.; Tuchagues, J.-P.; Vendier, L. Structural and Magnetic Study of a Trinuclear MnII-GdIII-MnIIComplex. *Eur. J. Inorg. Chem.* **2009**, *2009*, 3801−3806.
(23) Singh, S. K.; Pedersen, K. S.; Sigrist, M.; Thuesen, C. A.; Schau-Magnussen, M.; Mutka, H.; Piligkos, S.; Weihe, H.; Rajaraman, G.; Bendix, J. Angular dependence of the exchange interaction in fluoride-bridged Gd-III-Cr-III complexes. *Chem. Commun.* **2013**, *49*, 5583−5585.
(24) Cremades, E.; Gómez-Coca, S.; Aravena, D.; Alvarez, S.; Ruiz, E. Theoretical Study of Exchange Coupling in 3d-Gd Complexes: Large Magnetocaloric Effect Systems. *J. Am. Chem. Soc.* **2012**, *134*, 10532−10542.
(25) Langley, S. K.; Chilton, N. F.; Moubaraki, B.; Hooper, T.; Brechin, E. K.; Evangelisti, M.; Murray, K. S. Molecular coolers: The case for [CuII5GdIII4]. *Chem. Sci.* **2011**, *2*, 1166−1169.
(26) Zheng, Y.-Z.; Evangelisti, M.; Winpenny, R. E. P. Co-Gd phosphonate complexes as magnetic refrigerants. *Chem. Sci.* **2011**, *2*, 99−102.
(27) Karotsis, G.; Kennedy, S.; Teat, S. J.; Beavers, C. M.; Fowler, D. A.; Morales, J. J.; Evangelisti, M.; Dalgarno, S. J.; Brechin, E. K. [MnIII4LnIII4] Calix[4]arene Clusters as Enhanced Magnetic Coolers and Molecular Magnets. *J. Am. Chem. Soc.* **2010**, *132*, 12983−12990.
(28) Dermitzaki, D.; Lorusso, G.; Raptopoulou, C. P.; Psycharis, V.; Escuer, A.; Evangelisti, M.; Perlepes, S. P.; Stamatatos, T. C. Molecular Nanoscale Magnetic Refrigerants: A Ferrimagnetic {CuII15GdIII7} Cagelike Cluster from the Use of Pyridine-2,6-dimethanol. *Inorg. Chem.* **2013**, *52*, 10235−10237.
(29) Peng, J.-B.; Zhang, Q.-C.; Kong, X.-J.; Zheng, Y.-Z.; Ren, Y.-P.; Long, L.-S.; Huang, R.-B.; Zheng, L.-S.; Zheng, Z. High-Nuclearity 3d-4f Clusters as Enhanced Magnetic Coolers and Molecular Magnets. *J. Am. Chem. Soc.* **2012**, *134*, 3314−3317.
(30) Birk, T.; Pedersen, K. S.; Thuesen, C. A.; Weyhermüller, T.; Schau-Magnussen, M.; Piligkos, S.; Weihe, H.; Mossin, S.; Evangelisti, M.; Bendix, J. Fluoride Bridges as Structure-Directing Motifs in 3d-4f Cluster Chemistry. *Inorg. Chem.* **2012**, *51*, 5435−5443.
(31) Hanninen, M. M.; Mota, A. J.; Sillanpaa, R.; Dey, S.; Velmurugan, G.; Rajaraman, G.; Colacio, E. Magneto-structural properties and theoretical studies of a family of simple heterodinuclear phenoxide/alkoxide bridged mniiilniii complexes: on the nature of the magnetic exchange and magnetic anisotropy. *Inorg. Chem.* **2018**, *57*, 3683−3698.
(32) Zheng, Y.-Z.; Pineda, E. M.; Helliwell, M.; Winpenny, R. E. P. MnII-GdIII Phosphonate Cages with a Large Magnetocaloric Effect. *Chem. - Eur. J.* **2012**, *18*, 4161−4165.
(33) Chen, Y. C.; Guo, F. S.; Liu, J. L.; Leng, J. D.; Vrabel, P.; Orendac, M.; Prokleska, J.; Sechovsky, V.; Tong, M. L. Switching of the Magnetocaloric Effect of Mn-II Glycolate by Water Molecules. *Chem. - Eur. J.* **2014**, *20*, 3029−3035.
(34) Guo, F.-S.; Chen, Y.-C.; Liu, J.-L.; Leng, J.-D.; Meng, Z.-S.; Vrabel, P.; Orendac, M.; Tong, M.-L. A large cryogenic magneto-caloric effect exhibited at low field by a 3D ferromagnetically coupled Mn(ii)-Gd(iii) framework material. *Chem. Commun.* **2012**, *48*, 12219−12221.
(35) Moreno Pineda, E.; Chilton, N. F.; Tuna, F.; Winpenny, R. E.; McInnes, E. J. Systematic Study of a Family of Butterfly-Like {M2Ln2} Molecular Magnets (M= MgII, MnIII, CoII, NiII, and CuII; Ln= YIII, GdIII, TbIII, DyIII, HoIII, and ErIII). *Inorg. Chem.* **2015**, *54*, 5930−5941.
(36) Colacio, E.; Ruiz, J.; Lorusso, G.; Brechin, E. K.; Evangelisti, M. A ferromagnetically coupled diphenoxo-bridged Gd 3+-Mn 2+ dinuclear complex with a large magneto-caloric effect. *Chem. Commun.* **2013**, *49*, 3845−3847.
(37) Mereacre, V.; Lan, Y.; Clerac, R.; Ako, A. M.; Hewitt, I. J.; Wernsdorfer, W.; Buth, G.; Anson, C. E.; Powell, A. K. Family of Mn(III)(2)Ln(2)(mu(4)-O) compounds: syntheses, structures, and magnetic properties. *Inorg. Chem.* **2010**, *49*, 5293−302.
(38) Mereacre, V.; Akhtar, M. N.; Lan, Y.; Ako, A. M.; Clerac, R.; Anson, C. E.; Powell, A. K. Structures and magnetic properties of Mn(III)(4)Ln(III)(4) aggregates with a "square-in-square" topology. *Dalton Trans* **2010**, *39*, 4918−27.
(39) Mereacre, V. M.; Ako, A. M.; Clérac, R.; Wernsdorfer, W.; Filoti, G.; Bartolomé, J.; Anson, C. E.; Powell, A. K. A Bell-Shaped Mn11Gd2 Single-Molecule Magnet. *J. Am. Chem. Soc.* **2007**, *129*, 9248−9249.
(40) Chesman, A. S.; Turner, D. R.; Berry, K. J.; Chilton, N. F.; Moubaraki, B.; Murray, K. S.; Deacon, G. B.; Batten, S. R. Ln(III)2Mn(III)2 heterobimetallic "butterfly" complexes displaying antiferromagnetic coupling (Ln = Eu, Gd, Tb, Er). *Dalton Trans* **2012**, *41*, 11402−12.
(41) Benelli, C.; Murrie, M.; Parsons, S.; Winpenny, R. E. P. Synthesis, structural and magnetic characterisation of a new Mn-Gd pivalate: preparation from a pre-formed hexanuclear cluster†. *J. Chem. Soc., Dalton Trans.* **1999**, 4125−4126.
(42) Liu, J.; Ma, C.; Chen, H.; Hu, M.; Wen, H.; Cui, H.; Chen, C. The first heterometallic examples of 3d-4f heptanuclear [Mn(II)3Ln-(III)4] complexes with planar disc-like cores and diverse magnetic properties. *Dalton Trans* **2013**, *42*, 3787−90.
(43) Bag, P.; Chakraborty, A.; Rogez, G.; Chandrasekhar, V. Pentanuclear heterometallic {Mn(III)(2)Ln(3)} (Ln = Gd, Dy, Tb, Ho) assemblies in an open-book type structural topology: appearance of slow relaxation of magnetization in the Dy(III) and Ho(III) analogues. *Inorg. Chem.* **2014**, *53*, 6524−33.
(44) Chandrasekhar, V.; Bag, P.; Speldrich, M.; van Leusen, J.; Kogerler, P. Synthesis, structure, and magnetic properties of a new

DOI: 10.1021/acs.inorgchem.9b01503
Inorg. Chem. 2019, 58, 11927−11940

family of tetra-nuclear {Mn2(III)Ln2}(Ln = Dy, Gd, Tb, Ho) clusters with an arch-type topology: single-molecule magnetism behavior in the dysprosium and terbium analogues. *Inorg. Chem.* **2013**, *52*, 5035−44.
(45) Chandrasekhar, V.; Pandian, B. M.; Boomishankar, R.; Steiner, A.; Clerac, R. Synthesis, structure and magnetic properties of linear heterobimetallic trinuclear Mn2Ln (Ln = Eu, Gd, Dy) complexes. *Dalton Trans* **2008**, 5143−5.
(46) Papatriantafyllopoulou, C.; Abboud, K. A.; Christou, G. Carboxylate-free Mn(III)2Ln(III)2 (Ln = lanthanide) and Mn(III)-2Y(III)2 complexes from the use of (2-hydroxymethyl)pyridine: analysis of spin frustration effects. *Inorg. Chem.* **2011**, *50*, 8959−66.
(47) Saha, A.; Thompson, M.; Abboud, K. A.; Wernsdorfer, W.; Christou, G. Family of double-cubane Mn4Ln2 (Ln = Gd, Tb, Dy, Ho) and Mn4Y2 complexes: a new Mn4Tb2 single-molecule magnet. *Inorg. Chem.* **2011**, *50*, 10476−85.
(48) Chilton, N. F.; Langley, S. K.; Moubaraki, B.; Murray, K. S. Synthesis, structural and magnetic studies of an isostructural family of mixed 3d/4f tetranuclear 'star' clusters. *Chem. Commun. (Cambridge, U. K.)* **2010**, *46*, 7787−9.
(49) Li, M.; Ako, A. M.; Lan, Y.; Wernsdorfer, W.; Buth, G.; Anson, C. E.; Powell, A. K.; Wang, Z.; Gao, S. New heterometallic [Mn(III)(4)Ln(III)(4)] wheels incorporating formate ligands. *Dalton Trans* **2010**, *39*, 3375−7.
(50) Shiga, T.; Hoshino, N.; Nakano, M.; Nojiri, H.; Oshio, H. Syntheses, structures, and magnetic properties of manganese-lanthanide hexanuclear complexes. *Inorg. Chim. Acta* **2008**, *361*, 4113−4117.
(51) Mukherjee, S.; Daniels, M. R.; Bagai, R.; Abboud, K. A.; Christou, G.; Lampropoulos, C. A variety of new tri- and tetranuclear Mn-Ln and Fe-Ln (Ln = lanthanide) complexes. *Polyhedron* **2010**, *29*, 54−65.
(52) Khan, A.; Lan, Y.; Kostakis, G. E.; Anson, C. E.; Powell, A. K. Using the flexible ligand bis(2-hydroxyethyl)amino-tris (hydroxymethyl)methane ("bis-tris") to access a family of 3d-4f Mn(III)4Ln4 complexes. *Dalton Trans* **2012**, *41*, 8333−9.
(53) Waldmann, O.; Ako, A. M.; Güdel, H. U.; Powell, A. K. Assessment of the anisotropy in the molecule Mn19 with a high-spin ground state S= 83/2 by 35 GHz electron paramagnetic resonance. *Inorg. Chem.* **2008**, *47*, 3486−3488.
(54) Liu, J. L.; Chen, Y. C.; Li, Q. W.; Gomez-Coca, S.; Aravena, D.; Ruiz, E.; Lin, W. Q.; Leng, J. D.; Tong, M. L. Two 3d-4f nanomagnets formed via a two-step in situ reaction of picolinaldehyde. *Chem. Commun.* **2013**, *49*, 6549−6551.
(55) Rajeshkumar, T.; Annadata, H. V.; Evangelisti, M.; Langley, S. K.; Chilton, N. F.; Murray, K. S.; Rajaraman, G. Theoretical Studies on Polynuclear {(Cu5GdnIII)-Gd-II} Clusters (n = 4, 2): Towards Understanding Their Large Magnetocaloric Effect. *Inorg. Chem.* **2015**, *54*, 1661−1670.
(56) Gupta, S. K.; Dar, A. A.; Rajeshkumar, T.; Kuppuswamy, S.; Langley, S. K.; Murray, K. S.; Rajaraman, G.; Murugavel, R. Discrete {(Gd4M)-M-III} (M = Gd-III or Co-II) pentanuclear complexes: a new class of metal-organophosphate molecular coolers. *Dalton Trans* **2015**, *44*, 5961−5965.
(57) Singh, S. K.; Rajaraman, G. Decisive interactions that determine ferro/antiferromagnetic coupling in {3d-4f} pairs: a case study on dinuclear {V(IV)-Gd(III)} complexes. *Dalton Trans* **2013**, *42*, 3623−3630.
(58) Singh, S. K.; Tibrewal, N. K.; Rajaraman, G. Density functional studies on dinuclear {(NiGdIII)-Gd-II} and trinuclear {(NiGdNiII)-Gd-II-Ni-III} complexes: magnetic exchange and magneto-structural maps. *Dalton Trans* **2011**, *40*, 10897−10906.
(59) Rajeshkumar, T.; Singh, S. K.; Rajaraman, G. A computational perspective on magnetic coupling, magneto-structural correlations and magneto-caloric effect of a ferromagnetically coupled {Gd-III-Gd-III} pair. *Polyhedron* **2013**, *52*, 1299−1305.
(60) Liu, J. L.; Lin, W. Q.; Chen, Y. C.; Gomez-Coca, S.; Aravena, D.; Ruiz, E.; Leng, J. D.; Tong, M. L. Cu-II-Gd-III Cryogenic Magnetic Refrigerants and Cu8Dy9 Single-Molecule Magnet Generated by In Situ Reactions of Picolinaldehyde and Acetylpyridine: Experimental and Theoretical Study. *Chem. - Eur. J.* **2013**, *19*, 17567−17577.
(61) Zou, H. H.; Sheng, L. B.; Liang, F. P.; Chen, Z. L.; Zhang, Y. Q. Experimental and theoretical investigations of four 3d-4f butterfly single-molecule magnets. *Dalton Trans* **2015**, *44*, 18544−52.
(62) Pedersen, K. S.; Lorusso, G.; Morales, J. J.; Weyhermuller, T.; Piligkos, S.; Singh, S. K.; Larsen, D.; Schau-Magnussen, M.; Rajaraman, G.; Evangelisti, M.; Bendix, J. Fluoride-Bridged {Gd-III M-3(III) (2)} (M= Cr, Fe, Ga) Molecular Magnetic Refrigerants**. *Angew. Chem., Int. Ed.* **2014**, *53*, 2394−2397.
(63) Palacios, M. A.; McLellan, R.; Beavers, C. M.; Teat, S. J.; Weihe, H.; Piligkos, S.; Dalgarno, S. J.; Brechin, E. K. Facile Interchange of 3d and 4f Ions in Single-Molecule Magnets: Stepwise Assembly of [Mn4],[Mn3Ln] and [Mn2Ln2] Cages within Calix [4] arene Scaffolds. *Chem. - Eur. J.* **2015**, *21*, 11212−11218.
(64) Berg, N.; Rajeshkumar, T.; Taylor, S. M.; Brechin, E. K.; Rajaraman, G.; Jones, L. F. What Controls the Magnetic Interaction in bis-mu-Alkoxo MnIII Dimers? A Combined Experimental and Theoretical Exploration. *Chem. - Eur. J.* **2012**, *18*, 5906−5918.
(65) Langley, S. K.; Moubaraki, B.; Murray, K. S. Heterometallic Tetranuclear {Mn2IIILn2III} n 1D Coordination Polymers: Employing Sulfonate Ligands as Connecting Groups. *Aust. J. Chem.* **2014**, *67*, 1601−1606.
(66) Noodleman, L. Valence Bond Description of Anti-Ferromagnetic Coupling in Transition-Metal Dimers. *J. Chem. Phys.* **1981**, *74*, 5737−5743.
(67) Frisch, M. J.; Trucks, G. W.; Schlegel, H. B.; Scuseria, G. E.; Robb, M. A.; Cheeseman, J. R.; Scalmani, G.; Barone, V.; Mennucci, B.; Petersson, G. A.; Nakatsuji, H.; Caricato, M.; Li, X.; Hratchian, H. P.; Izmaylov, A. F.; Bloino, J.; Zheng, G.; Sonnenberg, J. L.; Hada, M.; Ehara, M.; Toyota, K.; Fukuda, R.; Hasegawa, J.; Ishida, M.; Nakajima, T.; Honda, Y.; Kitao, O.; Nakai, H.; Vreven, T.; Montgomery, J. A., Jr.; Peralta, J. E.; Ogliaro, F.; Bearpark, M. J.; Heyd, J.; Brothers, E. N.; Kudin, K. N.; Staroverov, V. N.; Kobayashi, R.; Normand, J.; Raghavachari, K.; Rendell, A. P.; Burant, J. C.; Iyengar, S. S.; Tomasi, J.; Cossi, M.; Rega, N.; Millam, N. J.; Klene, M.; Knox, J. E.; Cross, J. B.; Bakken, V.; Adamo, C.; Jaramillo, J.; Gomperts, R.; Stratmann, R. E.; Yazyev, O.; Austin, A. J.; Cammi, R.; Pomelli, C.; Ochterski, J. W.; Martin, R. L.; Morokuma, K.; Zakrzewski, V. G.; Voth, G. A.; Salvador, P.; Dannenberg, J. J.; Dapprich, S.; Daniels, A. D.; Farkas, Ö.; Foresman, J. B.; Ortiz, J. V.; Cioslowski, J.; Fox, D. J. *Gaussian 09*; Gaussian, Inc.: Wallingford, CT, USA, 2009.
(68) Becke, A. D. Density-Functional Thermochemistry. 3. The Role of Exact Exchange. *J. Chem. Phys.* **1993**, *98*, 5648−5652.
(69) Schafer, A.; Huber, C.; Ahlrichs, R. Fully Optimized Contracted Gaussian-Basis Sets of Triple Zeta Valence Quality for Atoms Li to Kr. *J. Chem. Phys.* **1994**, *100*, 5829−5835.
(70) Cundari, T. R.; Stevens, W. J. Effective Core Potential Methods for the Lanthanides. *J. Chem. Phys.* **1993**, *98*, 5555−5565.
(71) Borras-Almenar, J. J.; Clemente-Juan, J. M.; Coronado, E.; Tsukerblat, B. S. MAGPACK(1) a package to calculate the energy levels, bulk magnetic properties, and inelastic neutron scattering spectra of high nuclearity spin clusters. *J. Comput. Chem.* **2001**, *22*, 985−991.
(72) Chilton, N. F.; Anderson, R. P.; Turner, L. D.; Soncini, A.; Murray, K. S. PHI: A powerful new program for the analysis of anisotropic monomeric and exchange-coupled polynuclear d- and f-block complexes. *J. Comput. Chem.* **2013**, *34*, 1164−1175.
(73) Vignesh, K. R.; Langley, S. K.; Moubaraki, B.; Murray, K. S.; Rajaraman, G. Understanding the Mechanism of Magnetic Relaxation in Pentanuclear {MnIVMnIII2LnIII2} Single-Molecule Magnets. *Inorg. Chem.* **2018**, *57*, 1158−1170.
(74) Chakraborty, A.; Goura, J.; Kalita, P.; Swain, A.; Rajaraman, G.; Chandrasekhar, V. Heterometallic 3d-4f single molecule magnets containing diamagnetic metal ions. *Dalton Trans* **2018**, *47*, 8841−8864.

DOI: 10.1021/acs.inorgchem.9b01503
Inorg. Chem. 2019, 58, 11927−11940

(75) Vignesh, K. R.; Langley, S. K.; Murray, K. S.; Rajaraman, G. Exploring the influence of diamagnetic ions on the mechanism of magnetization relaxation in {CoIII2LnIII2}(Ln= Dy, Tb, Ho)"butterfly" complexes. *Inorg. Chem.* **2017**, *56*, 2518−2532.
(76) Stamatatos, T. C.; Teat, S. J.; Wernsdorfer, W.; Christou, G. Enhancing the quantum properties of manganese-lanthanide single-molecule magnets: observation of quantum tunneling steps in the hysteresis loops of a {Mn12Gd} cluster. *Angew. Chem., Int. Ed.* **2009**, *48*, 521−4.
(77) Barros, W. P.; Inglis, R.; Nichol, G. S.; Rajeshkumar, T.; Rajaraman, G.; Piligkos, S.; Stumpf, H. O.; Brechin, E. K. From antiferromagnetic to ferromagnetic exchange in a family of oxime-based Mn III dimers: a magneto-structural study. *Dalton Trans* **2013**, *42*, 16510−16517.

DOI: 10.1021/acs.inorgchem.9b01503
Inorg. Chem. 2019, 58, 11927−11940